Compressive Properties of Soybean Oil-Based Polymers at Quasi-Static and Dynamic Strain Rates

Bo Song,[1] Weinong Chen,[1] Zengshe Liu,[2] Sevim Z. Erhan[2]

[1]*Department of Aerospace and Mechanical Engineering, The University of Arizona, Tucson, Arizona 85721*
[2]*NCAUR, ARS, USDA, Peoria, Illinois 61604*

Received 13 August 2004; accepted 7 April 2005
DOI 10.1002/app.22627
Published online 19 December 2005 in Wiley InterScience (www.interscience.wiley.com).

ABSTRACT: Quasi-static and dynamic compressive properties of three soybean oil-based polymeric materials, which were made through the reaction of epoxidized soybean oil with diamine compounds, have been determined. Quasi-static properties were determined with an MTS 810 hydraulically driven testing machine, whereas dynamic experiments were conducted with a split Hopkinson pressure bar (SHPB) modified for low-impedance material testing. All three materials were capable of deforming to very large strains, with significant nonlinear stress–strain response. Their compressive behaviors were strain-rate sensitive with distinctive rate sensitivities. On the basis of the experimental results at various strain rates, a compressive one-dimensional stress–strain material model with strain-rate effects was developed to describe the experimental results for all three materials under both quasi-static and dynamic loading conditions. © 2005 Wiley Periodicals, Inc. J Appl Polym Sci 99: 2759–2770, 2006

Key words: soybean oil-based polymers; split Hopkinson pressure bar (SHPB); stress–strain curve; strain rate; compressive properties

INTRODUCTION

Recently, there has been a growing interest in the development of polymers obtained from biodegradable and environmentally friendly resources. One of these resources is soybean oil. Besides the major use in food products, soybean oil has been used in nonfood applications, including lubricants, plastics, coatings, fuel, inks, and chemical intermediates.[1–5] It was used as a plasticizer for polyvinyl chloride (PVC) compounds, chlorinated rubber, and polyvinyl alcohol (PVA) emulsions, in the past. Recently, epoxidized soybean oil (ESO) has been reacted with diamine compounds to produce three new soybean oil-based materials, which are studied in this paper.

The expected applications of these materials are in the automotive industry, civil engineering, construction industry, and sports equipment industry. However, as a class of new materials, knowledge about their mechanical properties at quasi-static and dynamic strain rates is scarce, and thus, it is desirable to understand the mechanical properties before the projected strain-rate-dependent load-bearing applications. Systematic research is needed to experimentally determine their mechanical properties and to analytically develop realistic material models for numerical simulations and design optimizations. Since material models need reliable experimental data to determine the material constants and to check the accuracy of the models over the ranges of their applications, detailed stress–strain curves for such materials at various strain rates must be accurately determined under valid experimental conditions.

Under quasi-static loading conditions, standard experimental techniques can be directly employed to determine the mechanical properties of those materials.[6,7] However, it is much more challenging to determine the mechanical properties under dynamic loadings because most dynamic experimental techniques are not adequate to load the soft materials at both large strains and high strain rates. For example, dynamic viscoelastic properties of the materials prepared by curing ESO with various cyclic acid anhydrides in the presence of tertiary amines by Gerbase et al.,[8] and of soybean oil-based composites with and without fibrous filler prepared by Xu et al.[9] have been investigated. This type of experimentation determines the storage modulus and loss modulus of polymers at very small strains instead of large strains. For the purpose of dynamic material model development, detailed stress–strain curves over wide ranges of strains and strain rates are necessary. The split Hopkinson pressure bar (SHPB), originally developed by Kolsky,[10] has been widely used and modified to determine families of stress–strain curves as a function of strain rates for a variety of engineering materials, including metals,[11,12] composites,[13–15] and soft materials.[16] It is noted that, when the specimen in a SHPB is

Correspondence to: W. Chen (wchen@purdue.edu).

TABLE I
Descriptions of the Three Soybean Oil-Based Polymeric Materials

Sample code	ESO (g)[a]	Curing agent (g)[a]			T_g (°C)
		TETA	DETA	TETA	
ESOT-I	140.6 (0.141)	40.3 (0.28)			7.84
ESOD	149.1 (0.149)		30.3 (0.29)		1.51
ESOT-II	152.3 (0.152)			27.5 (0.19)	0.22

[a] Values in parentheses indicate moles.

a soft material, such as the soybean oil-based polymeric materials in this research, the applicability of the conventional SHPB technique needs to be examined carefully before reliable dynamic experimental data can be produced.[16] Recent modifications on the conventional SHPB for soft material tests have resolved the issue of weak transmitted signals caused by drastic impedance mismatch between the soft specimen and the metal bars,[17–20] and have also ensured valid testing conditions (homogeneous deformation, dynamic stress equilibrium, and constant strain rate), which are not satisfied automatically during conventional SHPB tests.[16,21,22] In this research, a hydraulically driven materials testing system (MTS 810) and a modified SHPB for soft material testing were employed to obtain the quasi-static and dynamic compressive stress–strain curves of the soybean oil-based materials. On the basis of the experimental results at various strain rates under valid testing conditions, a nonlinear strain-rate-dependent material model has been developed through the combination of a strain–energy function and a relaxation function.

EXPERIMENTAL PROCEDURES

The materials for mechanical testing were made at National Center for Agricultural Utilization Research (UCAUR), Agricultural Research Service (ARS), US Department of Agriculture (USDA) (Peoria, IL), through the reaction of ESO with diamine compounds. The ESO was provided by Elf Atochem North America, Inc. (Philadelphia, PA). The curing agents, diethylenetriamine (DETA; 99%) and triethylenetetramine (TETA; tech 60%), were provided by Aldrich Chemical Company, Inc. (Milwaukee, WI). During processing, ESO was mixed thoroughly with the curing agent, TETA or DETA. The mixture was cured at 100°C for 24 h, and then at 120°C for 24 h. The components and their amounts in the mixtures are tabulated in Table I. The T_g's for these materials are 7.84, 1.51, and 0.22°C for ESOT-I, ESOD, and ESOT-II, respectively, which are also listed in Table I. It is noted that the T_g's are below room temperature where both quasi-static and dynamic experiments were conducted. The as-cured materials were made into sheets. Then, the specimens for quasi-static mechanical tests were cut into cylinders with a diameter of ~8.0 mm and a thickness of ~6.0 mm. Those for dynamic experiments were cylinders with the same diameter but a smaller thickness of ~2.8 mm, because thinner specimens are necessary to achieve dynamic stress equilibrium during the dynamic SHPB experiments for soft materials.[16,23]

Quasi-static compressive experiments were performed with a standard MTS 810 hydraulically driven materials testing system at room temperature. Since the aspect ratio (thickness-to-diameter ratio) of specimen for quasi-static experiments was small (<1.0), the friction between the specimen and the platen surfaces on the MTS became a concern. A thin layer of petroleum jelly was carefully applied on both surfaces of the specimen to minimize the friction. Furthermore, to evaluate the effects of using a thin specimen, we conducted quasi-static experiments at a constant strain rate (0.01 s^{-1}) for the ESOT-I, with various specimen thicknesses of 8.7, 5.6, and 2.8 mm, the results of which are shown in Figure 1. The resultant stress–strain curves nearly overlap on each other, indicating that the friction between the specimen and the platen surfaces may be neglected. This conclusion may also be extended to the other two materials (ESOD and ESOT-II) because of their similar compositions.

Quasi-static stress–strain curves were obtained at four strain rates (0.001, 0.01, 0.1, and 1.0 s^{-1}) for each of the three materials (ESOT-I, ESOD, and ESOT-II). At least two experiments at each quasi-static strain rate for each material were performed, the results of which were repeatable. The strain rate was varied through the control of hydraulic actuator moving velocity in displacement control mode (fixed crosshead velocity).

An SHPB modified with pulse-shapers and quartz piezoelectric force transducers at the University of Arizona was employed to investigate the dynamic compressive stress–strain curves of the three materials listed in Table I (ESOT-I, ESOD, and ESOT-II), at room temperature. A schematic of the modified SHPB setup is shown in Figure 2. When the specimen in a SHPB experiment is a soft material, the large impedance mismatch between the bars and the specimen produces difficulties to check the dynamic stress equilibrium in soft specimen. Quartz piezoelectric force

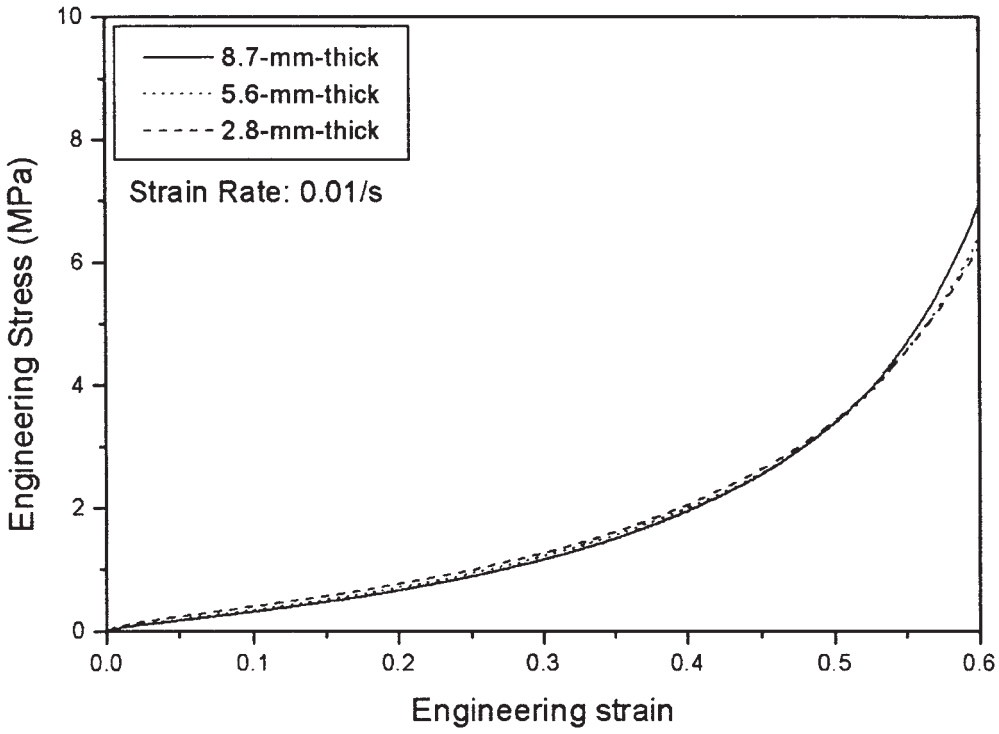

Figure 1 Comparison of stress–strain curves for ESOT-I specimens with various thicknesses at the same strain rate of 0.01 s^{-1}.

transducers in the modified SHPB setup were used to monitor the dynamic force equilibrium in the specimen, by determining the axial forces on the specimen end surfaces directly.[16,19] To ensure that the specimens deformed at nearly constant strain rates under dynamically equilibrated stresses, copper tubes with various diameters and lengths were used as pulse shapers to precisely control the profile of the loading (incident) pulse after trial experiments. Pulse-shaping in SHPB experiments has been demonstrated to be an effective method to achieve valid dynamic testing conditions.[24–27] The strain gauges used in this research had enough sensitivity to record the weak transmitted signals from the three materials accurately. Petroleum jelly was used to lubricate the interfaces between the specimen and bars, to minimize the interface friction.

A typical set of incident, reflected, and transmitted signals recorded by a digital oscilloscope with a sampling rate of 5 MHz through differential preamplifiers from such a pulse-shaped SHPB experiment on ESOT-I at a strain rate of 1650 s^{-1} are shown in Figure 3. The employment of pulse shaper modified the shape of the

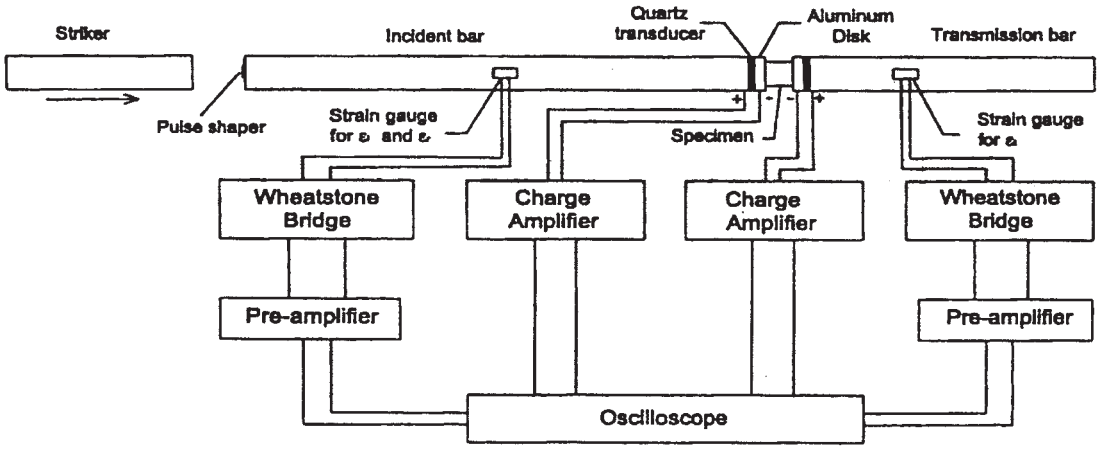

Figure 2 A schematic of the modified SHPB setup.

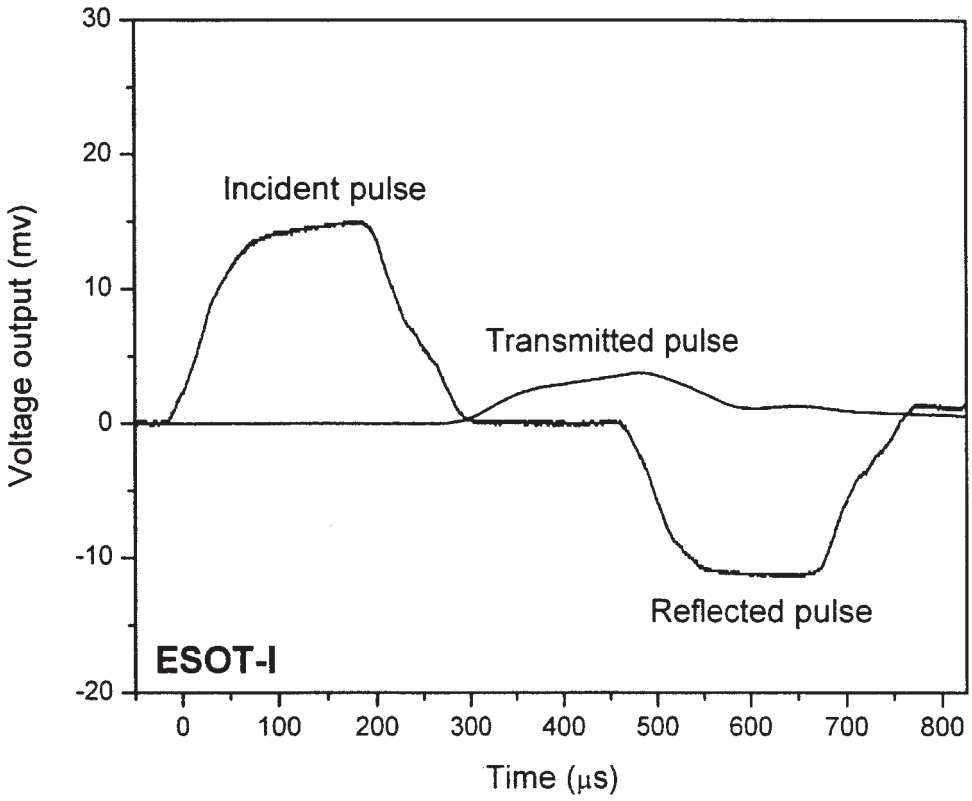

Figure 3 Typical incident, reflected, and transmitted signals from a pulse-shaped SHPB experiment on ESOT-I.

incident pulse, which is different from that obtained from a conventional SHPB experiment, to produce a nearly flat plateau in reflected signal shown in Figure 3. If the specimen is in dynamic stress equilibrium, the nearly flat plateau in reflected signal corresponds to a nearly constant strain rate during the dynamic experiment. Thus, the dynamic stress equilibrium becomes a critical factor for validity of the experimental results. Figure 4 shows the time history of dynamic stress equilibrium in the specimen. The relative error indicating nonequilibrium is described as[28]

$$R(t) = \left|\frac{\Delta\sigma(t)}{\sigma_{avg}(t)}\right| = 2\left|\frac{F_1 - F_2}{F_1 + F_2}\right| \qquad (1)$$

where $\Delta\sigma$ and σ_{avg} are difference and averaged values between the stresses at both ends of the specimen, respectively, and $F_1$and F_2 are axial forces at the front end (facing incident bar) and back end (facing transmission bar) of the specimen, respectively, as measured by the piezoelectric force transducers mounted near the specimen (Fig. 2). As shown in Figure 4, a dynamic stress equilibrium was achieved $\sim$50 μs after the front end was initially loaded, indicating that the specimen deformed under dynamically equilibrated stress over most of the duration ($>$ 300 μs) of the SHPB experiment, while the strain rate was kept as a constant. The valid experimental conditions (nearly constant strain-rate deformation under dynamically equilibrated stress) ensured that the resultant dynamic compressive stress–strain curves from such an experiment provide a reliable description of the dynamic mechanical response of the soft material along the loading axis.

Following the same procedure, dynamic SHPB experiments were conducted on the ESOT-I specimens at strain rates of 230, 530, and 1650 s^{-1}, on ESOD specimens at strain rates of 240, 580, and 1640 s^{-1}, and on ESOT-II specimens at strain rates of 240, 540, and 1630 s^{-1}, respectively. At least three repeatable experiments were performed at each strain rate, under dynamic loading conditions. The validity check was performed on each experiment to ensure the reliability and accuracy of the resultant stress–strain curves. The strain rate was varied through the variation of striker bar initial velocity and pulse shapers.

Unlike the isothermal deformation in specimens in quasi-static experiments, the specimen encountered adiabatic heating under dynamic loading, which may produce significant adiabatic temperature rise in specimen, during dynamic loading. Thus, the effects of the adiabatic temperature rise on the compressive properties are necessary to be addressed because significant temperature rise may lead to the softening in material properties. In this study, a T-type thermocouple with a very low thermal mass and a diameter of 75

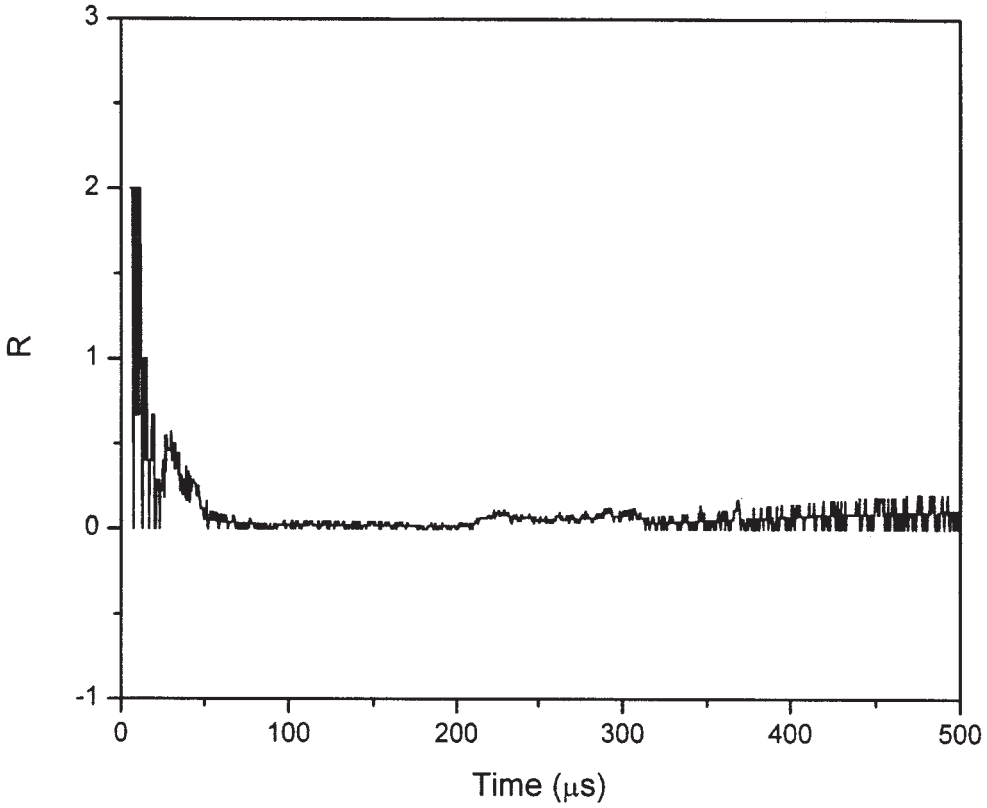

Figure 4 Dynamic equilibrium process in a specimen of ESOT-I.

μm was placed inside an ESOT-I specimen through a very small hole. The output signal from the thermocouple was recorded with the same oscilloscope, through a differential preamplifier. Figure 5 shows the variation of the temperature rise with the engineering strain in the ESOT-I specimen at the strain rate of 1650 s^{-1}. The temperature in specimen rose with the increasing engineering strain; however, it rose only ~2.75°C at the maximum engineering strain of 34.5%. The maximum temperature rise of <3°C at the very high strain rate of 1650 s^{-1} may not be considered to significantly affect the dynamic properties of the materials.

RESULTS

The quasi-static and dynamic compressive stress–strain curves at various strain rates for the three materials (ESOT-I, ESOD, and ESOT-II) are shown in Figure 6(a–c), respectively.

Since the effects of specimen thickness and temperature rise under dynamic loading are negligible as mentioned earlier, the only variable from quasi-static to dynamic experiments is the strain rate. Significant strain-rate effects were found on all three materials. To describe the strain-rate effects on the stress–strain responses more quantitatively, Table II lists the corresponding engineering stresses at the engineering strains of 5, 25, and 50% at various strain rates, for the three materials. In the range of quasi-static strain rates up to 0.1 s^{-1}, the stress for ESOT-I at a strain of 5% is less than 0.5 MPa. The stress at the same strain increases to 3.24 MPa at a strain rate of 1.0 s^{-1}, and to 26.64 MPa at a strain rate of 1650 s^{-1}, under dynamic loading conditions. When the engineering strain is 25%, the engineering stress increases from less than 2.0 MPa at quasi-static strain rates up to 0.1 s^{-1} to 55.64 MPa at the dynamic strain rate of 1650 s^{-1} through 7.74 MPa at the strain rate of 1.0 s^{-1}. Besides the strain-rate sensitivities of the stress values at certain strains, the shapes of the dynamic stress–strain curves are also different from those of quasi-static stress–strain curves. There is an initial nearly linear behavior, followed by a transitional nonlinear response and then a strain-hardening behavior, in the dynamic stress–strain curves. The stress level at the transitional strain increases with increasing strain rate. However, the initial linear behavior in quasi-static stress–strain curves is not significant except for the ones at the strain rate of 1.0 s^{-1}. In fact, the initial linear regions in the quasi-static stress–strain curves at the strain rates below 0.1 s^{-1} are hardly seen in Figure 6. It is found that the transitional behavior in the initial linear region occurred in the strain rate range of 0.1–1.0 s^{-1}. The mechanism of the transitional behavior will be investigated in future research. They will be-

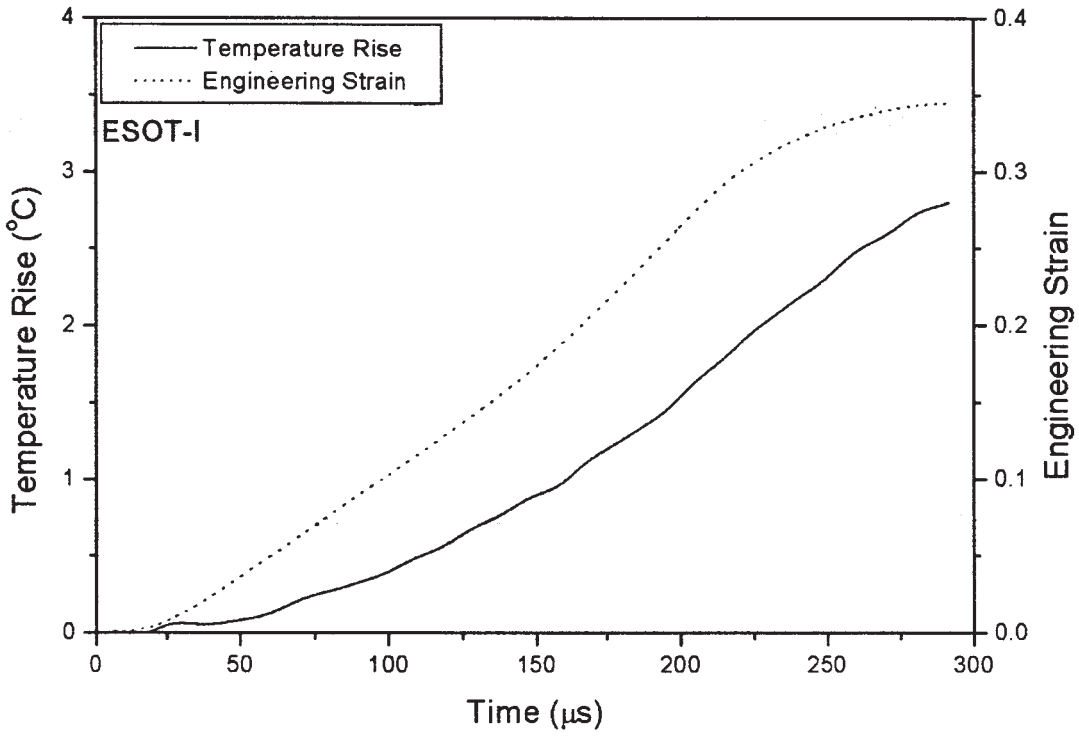

Figure 5 Temperature rise in a ESOT-I specimen with axial strain at the strain rate of 1650 s^{-1}.

come more visible when the quasi-static and dynamic curves are presented in separate figures, as shown in Figures 7–9. The nonlinear quasi-static stress–strain curves display strain-hardening behavior, with the tangential modulus increasing with increasing strains. An examination of the specimens after being compressed up to 30% of the maximum strain under dynamic loading conditions or 65% under quasi-static loading conditions reveals that all the specimens recovered with no or little residual strain, indicating the materials capabilities of deforming to large strains. The stress–strain curves for ESOD and ESOT-II qualitatively have shapes similar to those for ESOT-I, but are different quantitatively. At a strain of 5%, the ESOD sample had a stress of <0.25 MPa at quasi-static strain rates up to 0.1 s^{-1}, 3.24 MPa at a strain rate of 1.0 s^{-1}, 7.31 MPa at 240 s^{-1}, 12.35 MPa at 580 s^{-1}, and 15.53 MPa at 1640 s^{-1}. All the stress values are lower than the corresponding values at strain of 5% for ESOT-I. However, varying the ESO-to-agent ratio (i.e., ESOT-II) leads to complicated changes in the stress–strain curves, as indicated in Table II. The differences in the stress–strain curves for the three materials at various strain rates are considered to be the result of differences in material composition and crosslinking densities.

It is noted that the unloading parts in the stress–strain curves are not valid, although the unloading curve at the strain rate of 1650 s^{-1} was calculated and presented in Figure 6(a). The soft material under investigation clearly possesses a viscoelastic nature, where the strain lags behind applied stress. Furthermore, even when the strain starts to recover at a delayed time, the corresponding amplitudes of stress and strain rate (transmitted and reflected signals) are very small. Therefore, the recovery strain rate is very small compared to that when the specimen is compressed by the stress waves in the bars. Therefore, the dynamic unloading curve in Figure 6(a) was not obtained at a constant strain rate.

ONE-DIMENSIONAL RATE-DEPENDENT STRESS–STRAIN MODEL

As demonstrated by the experimental results, all these materials have nonlinear stress–strain responses with strong rate sensitivities. For the purposes of numerical simulations and design optimization, a simple but accurate material model is desired to describe the experimental results. Nonlinear large deformation behavior is conventionally described by strain energy functions. However, strong strain-rate sensitivity is a typical viscoelastic response. Strain–energy functions have been commonly used to describe the stress–strain behavior of rubbers at large strains, under quasi-static loading conditions.[29–32] A nonlinear viscoelastic constitutive equation based on the assumptions of nonlinear elasticity and linear viscoelasticity has been proposed to describe the rate-dependent mechanical behaviors for polymeric materials at small strains.[33]

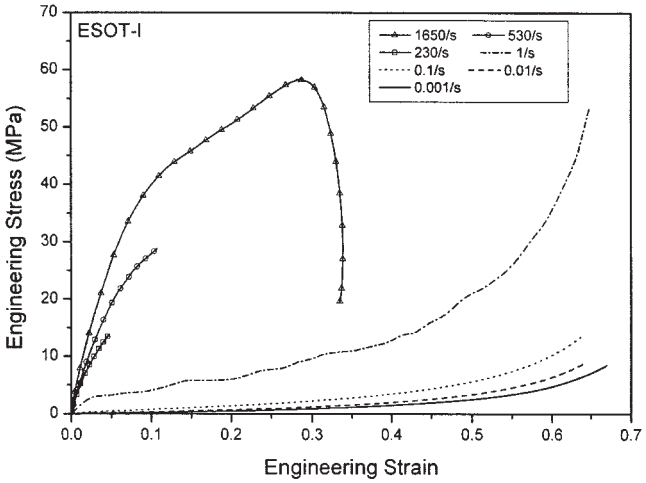

(a)

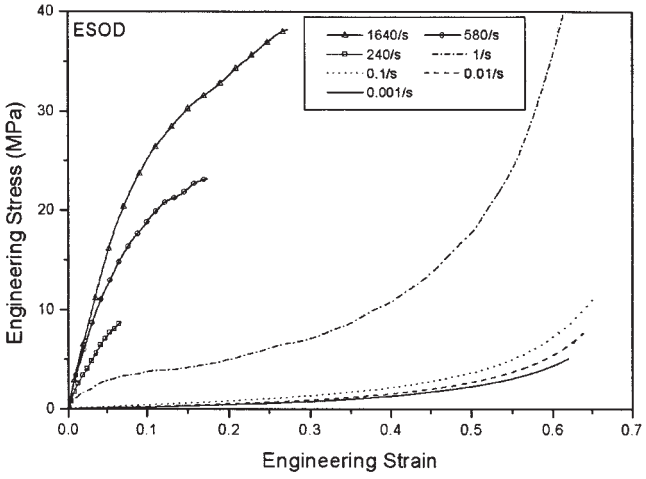

(b)

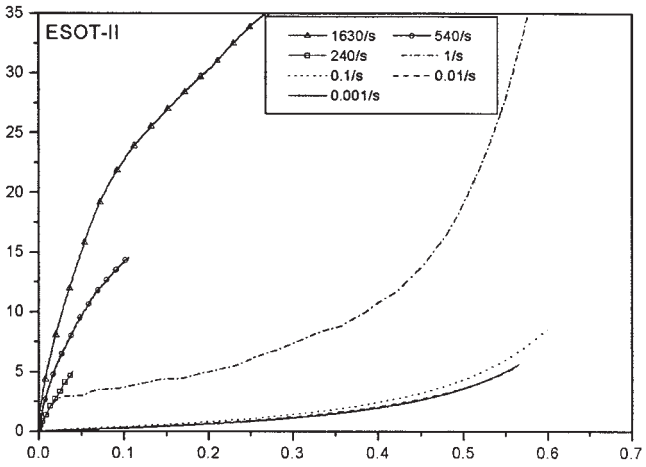

(c)

Figure 6 Engineering stress–strain curves of the three materials at various strain rates. (a) ESOT-I, (b) ESOD, and (c) ESOT-II.

TABLE II
Engineering Stresses at Various Engineering Strains (5, 25, and 50%) for the Three Materials

Sample code	Strain rate (s^{-1})	Engineering stress (MPa) at engineering strain of		
		5%	25%	50%
ESOT-I	0.001	0.12	0.75	2.81
	0.01	0.19	0.94	3.37
	0.1	0.44	1.75	5.70
	1	3.24	7.74	21.06
	230	13.59 (at 4.7%)	N/A	N/A
	530	19.16	N/A	N/A
	1650	26.64	55.64	N/A
ESOD	0.001	0.088	0.57	2.25
	0.01	0.12	0.69	2.68
	0.1	0.23	1.07	3.58
	1	2.87	6.12	17.74
	240	7.31	N/A	N/A
	580	12.35	N/A	N/A
	1640	15.53	37.02	N/A
ESOT-II	0.001	0.12	0.85	3.59
	0.01	0.14	0.88	3.61
	0.1	0.21	1.05	4.25
	1	2.97	6.05	19.11
	240	5.03 (at 3.9%)	N/A	N/A
	540	9.63	N/A	N/A
	1630	15.01	33.89	N/A

Recently, a novel strain-rate-dependent material model combining a strain energy function and a relaxation function for a viscoelastic solid has been developed to describe the strain-rate-dependent stress–strain behavior of an EPDM (ethylene–propylene–diene monomer) rubber in compression or tension.[34] A general form of the model is given by

$$\sigma = 2\left(\lambda^2 - \frac{1}{\lambda}\right)\left(\frac{\partial U}{\partial I_1} + \frac{1}{\lambda}\frac{\partial U}{\partial I_2}f_1(\dot{\varepsilon})\right) + f_2(\dot{\varepsilon})\int_{-\infty}^{t}\phi(t-\tau)\frac{d\varepsilon(\tau)}{d\tau}d\tau \quad (2)$$

where U is strain energy function; $I_1$and I_2 are strain invariants; $\phi(t)$ is a stress–relaxation function for a viscoelastic solid; $f_1(\dot{\varepsilon})$and $f_2(\dot{\varepsilon})$ represent the strain rate effects at large and small strains, respectively; λ is stretch ratio; and ε is engineering strain. Under one-dimensional compression, with the sign convention of compression as positive, the stretch ratio λ can be expressed as

$$\lambda = 1 - \varepsilon \quad (3)$$

The stretch rate $\dot{\lambda}$ can be expressed as

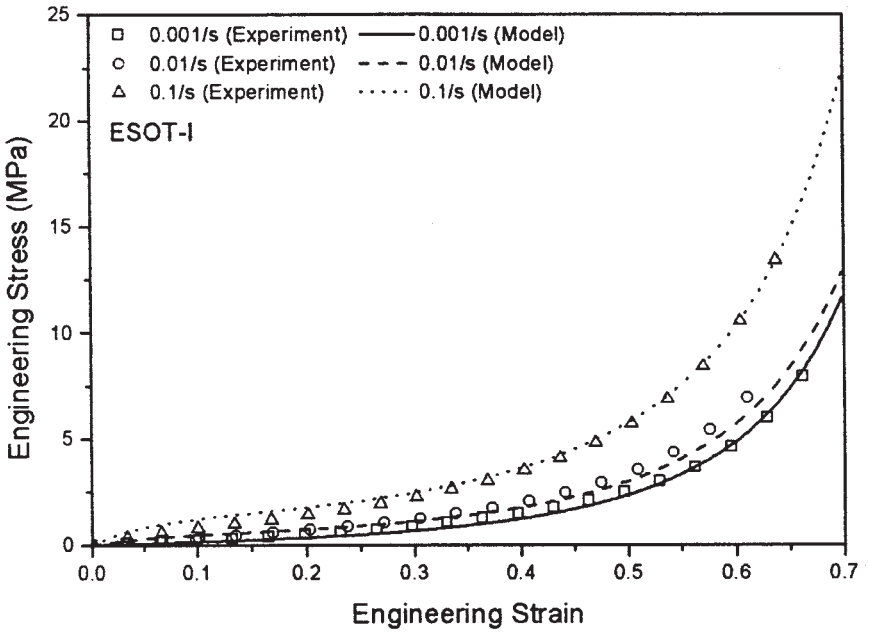

(a)

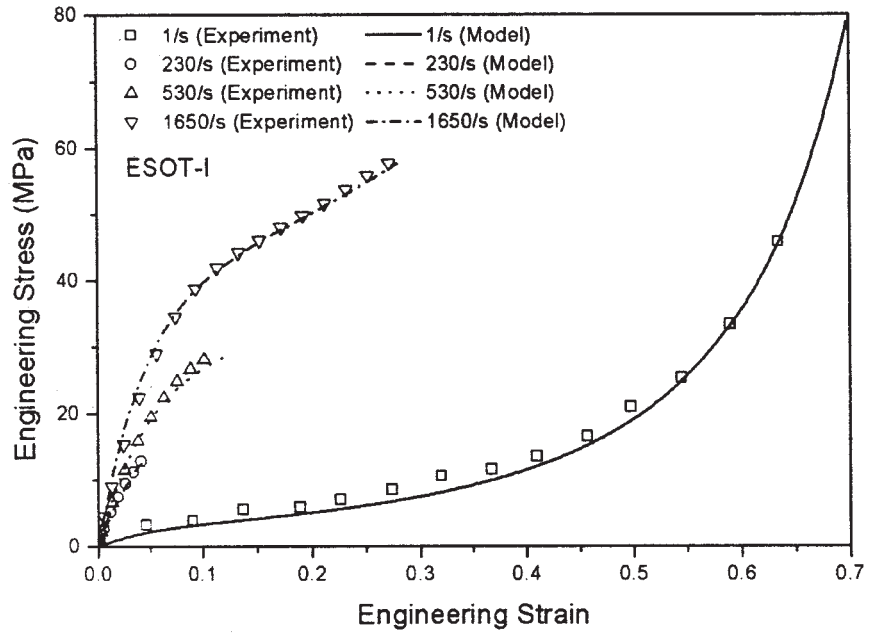

(b)

Figure 7 Comparison of true stress–engineering strain curves of ESOT-I determined by experiments and model. (a) at the strain rates up to 0.1 s^{-1} and (b) at the strain rates above 1.0 s^{-1}.

$$\dot{\lambda} = -\dot{\varepsilon} \tag{4}$$

where $\dot{\varepsilon}$ is engineering strain rate. The strain energy function, U, and the relaxation function, $\phi(t)$, have been proposed to take the forms[34]

$$U = C_1(I_1 - 3) + C_2(I_2 - 3) \tag{5}$$

$$\phi(t) = Ee^{-(t/\theta)} = Ee^{-(\varepsilon/\varepsilon_r)} \tag{6}$$

where C_1, C_2, E, and ε_r are constants; and

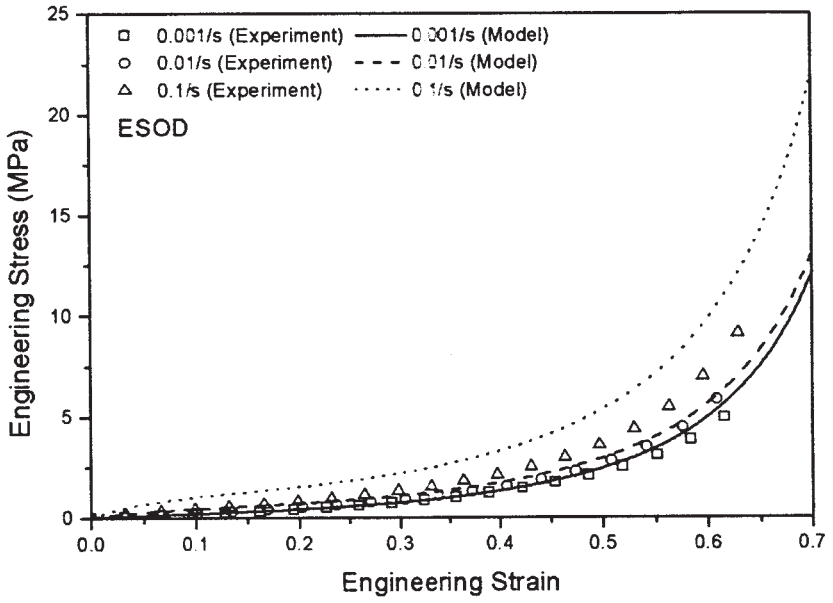

(a)

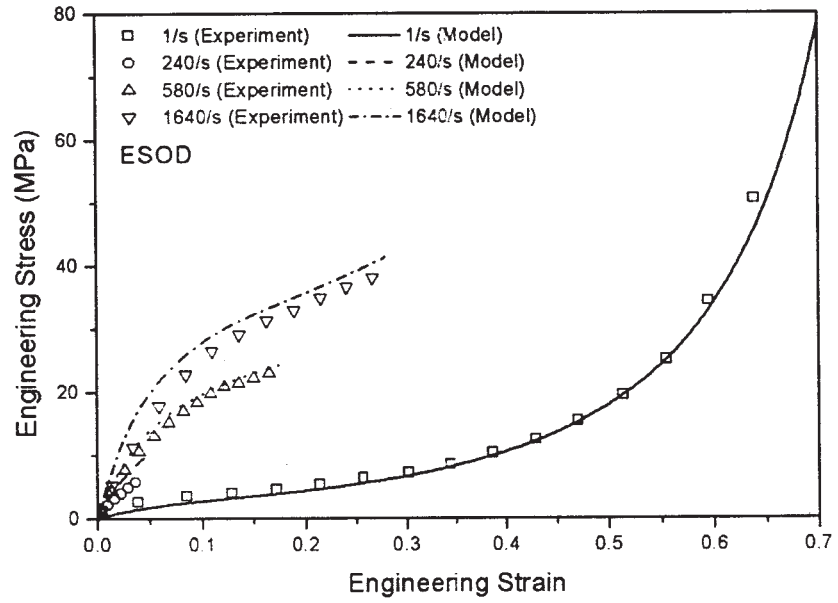

(b)

Figure 8 Comparison of true stress–engineering strain curves of ESOD determined by experiments and model. (a) at the strain rates up to 0.1 s^{-1} and (b) at the strain rates above 1.0 s^{-1}.

$$I_1 = \lambda^2 + \frac{2}{\lambda} \tag{7}$$

$$I_2 = \frac{1}{\lambda^2} + 2\lambda \tag{8}$$

$$\Theta = \frac{\varepsilon_r}{\dot{\varepsilon}} \tag{9}$$

Therefore, eq. (2) can be rewritten as[34]

$$\sigma = 2C_1\left(\lambda^2 - \frac{1}{\lambda}\right) + 2C_2\left(\lambda - \frac{1}{\lambda^2}\right)f_1(\dot{\varepsilon}) + f_2(\dot{\varepsilon})\sigma_r(1 - e^{-(\varepsilon/\varepsilon_r)}) \tag{10}$$

where $\sigma_r = E\varepsilon_r$

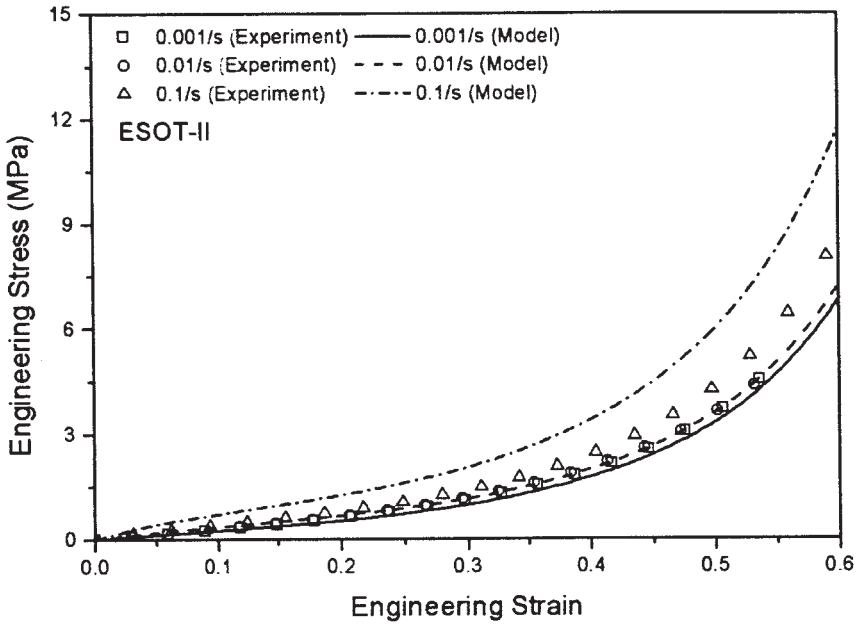

(a)

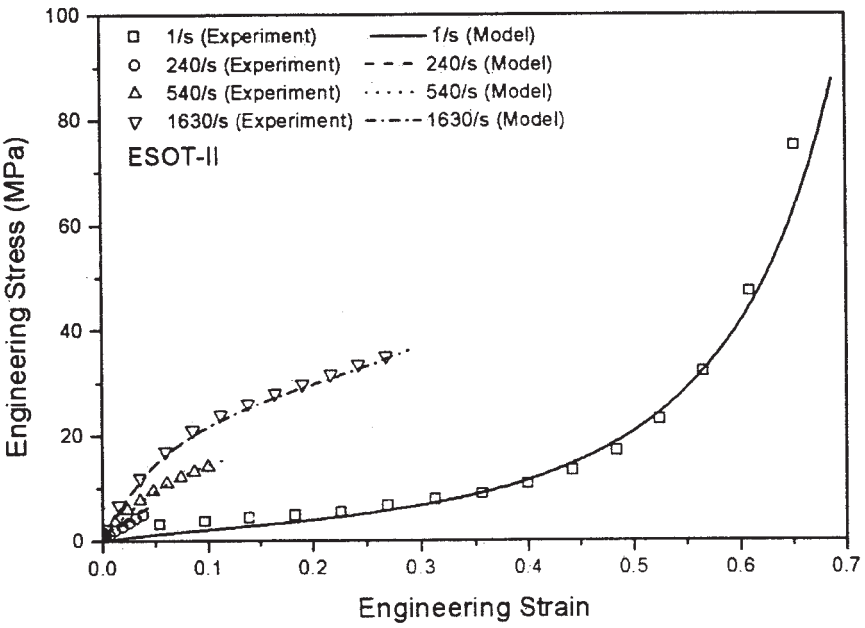

(b)

Figure 9 Comparison of true stress-engineering strain curves of ESOT-II determined by experiments and model. (a) at the strain rates up to 0.1 s^{-1} and (b) at the strain rates above 1.0 s^{-1}.

In this study, the form of eq. (10) was used to describe the strain-rate-dependent stress–strain behaviors of the three biomaterials. However, the curve-fitting results indicated $C_1 = 0$, which simplified the form without decreasing the accuracy of model. Moreover, the strain-rate-sensitive terms, $f_1(\dot{\varepsilon})$and $f_2(\dot{\varepsilon})$, took the forms

$$f_1(\dot{\varepsilon}) = C_3 + \frac{C_4}{1 + A_2\left(\frac{\dot{\varepsilon}}{\dot{\varepsilon}_0}\right)^{A_3}} \tag{11}$$

$$f_2(\dot{\varepsilon}) = a + b_1\left(\frac{\dot{\varepsilon}}{\dot{\varepsilon}_0}\right)^{\alpha} \quad (12)$$

where C_3, C_4, A_2, A_3, a, b_1, and α are constants and $\dot{\varepsilon}_0$ is a reference strain rate. Therefore, the new constitutive equation in compression for the three materials in this study can be expressed as

$$\sigma = \left[A_0 + \frac{A_1}{1 + A_2\left(\frac{\dot{\varepsilon}}{\dot{\varepsilon}_0}\right)^{A_3}}\right]\left(1-\varepsilon-\frac{1}{(1-\varepsilon)^2}\right) + \left[B_0+B_1\left(\frac{\dot{\varepsilon}}{\dot{\varepsilon}_0}\right)^{\alpha}\right](1-e^{-\varepsilon/\varepsilon_r}) \quad (13)$$

where

$$A_0 = 2C_3C_2 \quad (14)$$

$$A_1 = 2C_4C_2 \quad (15)$$

$$B_0 = a\sigma_r \quad (16)$$

$$B_1 = b_1\sigma_r. \quad (17)$$

It is noted that the stress (σ) in eq. (13) is true stress; however, the strain (ε) is engineering strain. The true stress can be converted into engineering stress (σ_{Eng}) under the assumption of constant volume compressive deformation

$$\sigma_{Eng} = \frac{\sigma}{1-\varepsilon}. \quad (18)$$

When the reference strain rate ($\dot{\varepsilon}_0$) is a normalized constant of 1.0 s^{-1}, eq. (13) can thus be expressed with engineering measurements

$$\sigma_{Eng} = \left[A_0 + \frac{A_1}{1 + A_2\dot{\varepsilon}^{A_3}}\right]\left(1 - \frac{1}{(1-\varepsilon)^3}\right) + [B_0 + B_1\dot{\varepsilon}^{\alpha}]\frac{1}{1-\varepsilon}(1 - e^{-\varepsilon/\varepsilon_r}). \quad (19)$$

The constitutive equation, eq. (19), indicates that the strain-rate-dependent stress–strain behavior of the materials may be separated into two portions: viscoelastic behavior at small strains and rate-sensitive hyperelastic behavior at large strains. When strain is very small, the hyperelastic stress is much less than viscoelastic stress so that only the viscoelastic behavior dominates the stress–strain behavior at small strains. However, at large strains, the hyperelastic stress will dominate the stress–strain behavior, and a constant viscoelastic stress is achieved.

TABLE III
Material Constants for the Model Described by Eq. (19)

	ESOT-I	ESOD	ESOT-II
A_0	−2.4105[a]	−2.4105[a]	−3.1805[a]
A_1	2.0849[a]	2.0849[a]	2.7279[a]
A_2		3.9746	
A_3		1.5613	
B_0	−0.2[a]	−0.1[a]	0[a]
B_1	2.7792[a]	2.0772[a]	1.1613[a]
α	0.3562	0.3466	0.3963
ε_r		0.05354	
$\dot{\varepsilon}_0$		1 s^{-1}	

[a] Values are in MPa.

The material constants in eq. (19) for ESOT-I, ESOD, and ESOT-II were determined by the quasi-static and dynamic experimental results, as tabulated in Table III. It is found that, besides the similar stress–strain profiles of the three materials, varying curing agent and ESO-to-agent ratio leads to various strain-rate sensitivities. Compared to the material constants for ESOT-I, changing into another curing agent but maintaining the same ESO-to-agent ratio in ESOD can only affect the strain-rate-sensitivities at small strains instead of at large strains; whereas employing the same curing agent but changing the ESO-to-agent ratio affects the strain-rate-sensitivities at both small and large strains.

Figures 7–9 show the comparisons of engineering stress–strain curves at both quasi-static and dynamic strain rates as described by the model, eq. (19), and the corresponding experimental results for ESOT-I, ESOD, and ESOT-II, respectively. The fact that the modeling results agree well with the corresponding experimental data except for the ones at the strain rate of 0.1 s^{-1} for ESOD and ESOT-II indicates that the one-dimensional stress–strain model developed in this research can describe the quasi-static and dynamic compressive behavior of the three materials at various strain rates such that the model may be applied in engineering design and optimization.

CONCLUSIONS

The quasi-static and dynamic compressive mechanical responses of three new soybean oil-based polymeric materials at various strain rates have been experimentally determined. The three materials showed significant strain-rate sensitivities and nonlinear behaviors. The strain-rate effects and the nonlinear behaviors are qualitatively the same for all three materials, but quantitatively different for different material compositions. A one-dimensional material model, combining a rate-dependent strain–energy function and a relaxation function in a viscoelastic framework, has been used to describe the strain-rate-dependent behavior of

the three materials at both large and small strains and at both high and low strain rates. This material model describes the experimental results well during loading.

References

1. Erhan, S. Z.; Bagby, M. O. J Am Oil Chem Soc 1991, 68, 635.
2. Erhan, S. Z.; Bagby, M. O.; Cunningham, H. W. J Am Oil Chem Soc 1992, 69, 251.
3. Dunn, R. O.; Bagby, M. O. J Am Oil Chem Soc 1995, 72, 895.
4. Dunn, R. O.; Shockley, M. W.; Bagby, M. O. J Am Oil Chem Soc 1996, 73, 1719.
5. Asadauskas, S.; Erhan, S. Z. J Am Oil Chem Soc 1999, 76, 313.
6. Li, F.; Larock, R. C. J Polym Sci Part A: Polym Phys 2000, 38, 2721.
7. Li, F.; Larock, R. C. J Polym Sci Part A: Polym Phys 2001, 39, 60.
8. Gerbase, A. E.; Petzhold, C. L.; Costa, A. P. O. J Am Oil Chem Soc 2002, 79, 797.
9. Xu, J.; Liu, Z.; Erhan, S. Z.; Carriere, C. J. J Am Oil Chem Soc 2002, 79, 593.
10. Kolsky, H. Proc Phys Soc London 1949, B62, 676.
11. Gray, G. T. In Metals Handbook: Mechanical Testing and Evaluation; ASTM: Materials Park, OH, 2000; Vol. 8, p 462.
12. Chen, W.; Song, B.; Frew, D. J.; Forrestal, M. J. Exp Mech 2003, 43, 20.
13. Hsiao, H. M.; Daniel, I. M.; Cordes, R. D. Exp Mech 1998, 38, 172.
14. Thiruppukuzhi, S. V.; Sun, C. T. Compos B Eng 1998, 29B, 535.
15. Song, B.; Chen, W.; Weerasooriya, T. J Compos Mater 2003, 37, 1723.
16. Chen, W.; Lu, F.; Frew, D. J.; Forrestal, M. J. ASME J Appl Mech 2002, 69, 214.
17. Zhao, H.; Gary, G.; Klepaczko, J. R. Int J Impact Eng 1997, 19, 319.
18. Sawas, O.; Brar, N. S.; Brockman, R. A. Exp Mech 1998, 38, 204.
19. Chen, W.; Lu, F.; Zhou, B. Exp Mech 2000, 40, 1.
20. Chen, W.; Zhang, B.; Forrestal, M. J. Exp Mech 1999, 39, 81.
21. Wu, X. J.; Gorham, D. A. J Phys IV France Colloque C3 (DYMAT 97) 1997, 7, 91.
22. Song, B.; Chen, W. J Eng Mater-T ASME 2003, 125, 294.
23. Song, B.; Chen, W. Exp Mech 2004, 44, 300.
24. Duffy, J.; Campbell, J. D.; Hawley, R. H. ASME J Appl Mech 1971, 37, 83.
25. Frantz, C. E.; Follansbee, P. S.; Wright, W. T. In Proceedings of the 8th International Conference on High Energy Rate Fabrication, San Antonio, TX; Berman, I., Schroeder, J. W., Eds.; 1984; p 229.
26. Nemat-Nasser, S.; Isaacs, J. B.; Starrett, J. E. Proc R Soc London Ser A 1991, 435, 371.
27. Frew, D. J.; Forrestal, M. J.; Chen, W. Exp Mech 2002, 42, 93.
28. Ravichandran, G.; Subhash, G. J Am Ceram Soc 1994, 77, 263.
29. Ward, I. M. In Mechanical Properties of Solid Polymers, 2nd ed.; Wiley: New York, 1983.
30. Spathis, G. D. J Appl Polym Sci 1991, 43, 613.
31. Chen, C.; Wang, Y. Polymer 1991, 38, 571.
32. Ogden, R. W.; Roxburgh, D. G. Proc R Soc London Ser A 1999, 455, 2861.
33. Wang, L. L.; Huang, D.; Gan, S. In Proceedings of the IUTAM Symposium on Constitutive Relation in High/Very High Strain Rates, Noda, Japan; Kawata, K., Shioiri, J., Eds.; 1995; p 137.
34. Song, B.; Chen, W.; Cheng, M. J Appl Polym Sci 2004, 92, 1553.